Research Square

Preprints are preliminary reports that have not undergone peer review.
They should not be considered conclusive, used to inform clinical practice,
or referenced by the media as validated information.

Temporal shift toward deterministic assembly shapes particle-associated core microbiome for cooperative nitrogen metabolism in small-scale greenhouse shrimp aquaculture systems

Ni Liu
Hainan University
Zhiyuan Yan
Hainan University
Yuxing Xie
Hainan University
Hao Long
Hainan University
Xiaoni Cai
Hainan University
Aiyou Huang
Hainan University
Yanhua Zeng
zengyanhua@hainanu.edu.cn

Hainan University
Zhenyu Xie
Hainan University

Research Article

Keywords: Small-scale greenhouse aquaculture, Deterministic assembly, Particle-associated microbiome, Functional convergence, Nitrogen metabolism

Posted Date: July 9th, 2026

DOI: https://doi.org/10.21203/rs.3.rs-9683146/v1

License: This work is licensed under a Creative Commons Attribution 4.0 International License.
Read Full License

Additional Declarations: No competing interests reported.

Abstract

In the near-closed greenhouse aquaculture systems for Pacific white shrimp, minimal water exchange necessitates microbial-mediated nutrient cycling to maintain water quality. However, whether efficient nitrogen removal relies on convergent functional pathways across geographically distinct systems remains unclear. We characterized water microbiomes from two major shrimp-farming regions in South China during early-to-mid (EM) and mid-to-late (ML) culture stages. 16S rRNA gene sequencing revealed significant differences in microbial community structure between regions and between free-living and particle-associated niches. Community assembly shifted from stochastic to deterministic processes over time, with homogeneous selection strongly structuring particle-associated communities in the ML stage. Despite taxonomic divergence, metagenomic analysis showed high functional convergence in ML-stage particle-associated microbiomes, with 459 out of 465 annotated KEGG pathways shared between regions. Key convergent functions essential for water purification included denitrification, dissimilatory nitrate reduction to ammonium (DNRA), assimilatory sulfate reduction, and thiosulfate oxidation. The potential for organic matter degradation was primarily driven by the predominance of glycoside hydrolases. Reconstruction of 101 medium/high-quality metagenome-assembled genomes (MAGs) and co-occurrence network analysis identified a core consortium, including *Demequina*, *Robiginitalea*, and *Nitrosomonas*. MAG-based network analysis revealed extensive positive interactions, with eight core MAGs linked to 78 others ($r > 0.8$). Notably, the 22 strongly correlated MAGs ($r > 0.9$) collectively encoded complete pathways for denitrification and DNRA, indicating functional cooperation within the microbial consortium. Our findings demonstrate that deterministic assembly shapes a functionally convergent and cooperative particle-associated core microbiome despite geographic variation in microbial composition, providing key insights for microbiome manipulation in near-closed aquaculture systems.

1. Introduction

Litopenaeus vannamei, commonly known as the Pacific white shrimp, is a globally significant aquaculture species valued for its rapid growth, broad salinity tolerance, and high nutritional quality (Li et al, 2017; Zhu et al, 2025). Over recent decades, its intensive farming has expanded considerably, with China emerging as the leading producer. In 2024, China's mariculture output of *L. vannamei* reached approximately 1.53 million tons, accounting for 82.5% of total national marine shrimp production, highlighting its pivotal economic importance (Fisheries bureau of the ministry of agriculture and rural affairs, 2025). This progress is largely attributable to continuous innovations in aquaculture practices, among which the small-scale greenhouse farming model represents a major advance (Chen et al, 2024). Originating in Rudong, Jiangsu Province, this model has been widely replicated across China due to its compelling advantages, including high productivity, improved survival rates, efficient water use and enhanced cost-effectiveness (Luo et al, 2021). Its successful implementation in regions such as Guangdong and Guangxi provinces has driven sustained production increases and operational success, establishing it as a pivotal innovation in modern shrimp farming.

Characterized by modular, greenhouse-enclosed water bodies, this system supports high-density, multi-batch cultivation throughout the year, largely independent of external climatic conditions (Chang et al, 2020). Unlike traditional open pond systems, which require large water volumes and frequent exchange that result in substantial water loss and environmental discharge, the small-scale greenhouse approach operates as a near-closed system with minimal water replacement. This design offers significant advantages in water conservation, land-use efficiency, and biosecurity (Wan, 2017). However, the high stocking densities and intensive feeding regimes lead to rapid accumulation of organic wastes and toxic metabolic byproducts (e.g, ammonia and nitrite). Without regular water exchange, maintaining suitable water quality depends entirely on internal biogeochemical processes, making it the critical factor determining system productivity and sustainability (Fang et al, 2023).

A defining feature of the small-scale greenhouse aquaculture system is its reliance on continuous probiotic supplementation and carbon source addition to maintain a high carbon-to-nitrogen (C/N) ratio. This promotes the proliferation of heterotrophic bacteria, which drives efficient nitrogen removal and thus allows for minimal water exchange, mirroring the water quality regulation achieved in Biofloc technology (BFT) systems (Wani et al, 2025; Yu et al, 2023). However, a critical distinction exists: while BFT systems typically yield protein-rich bioflocs (20%–50% crude protein) that serve as supplementary feed, the suspended particles in small-scale greenhouse systems exhibit a much lower crude protein content (approximately 2.5%) and are primarily composed of crude ash (Emerenciano et al, 2021; Huang et al, 2025; Li et al, 2024a). This difference arises from the substantial suspended sediment load in small-scale greenhouse systems, which contributes to suspended particle formation through the combined effects of intense aeration, shrimp bioturbation, and aquaculture waste accumulation (Joyni et al, 2011). Consequently, microbial communities in these systems likely exhibit higher abundance and play more critical functional roles compared to those in conventional aquaculture modes (e.g, higher-place pond mode and outdoor earth-pond mode), due to the persistent sediment-derived particles and limited water exchange (Huang et al, 2024a). Nevertheless, despite the central role of microbes in maintaining system stability and mediating water purification, research on the composition, dynamics, and functional mechanisms of these microbial communities remains limited and has not kept pace with industry development.

Growing recognition of the ecological significance of microbes has spurred recent research into the dynamics and functional traits of microbial communities in small-scale greenhouse aquaculture systems of *L. vannamei*. Temporal variations in both environmental and intestinal microbiota have been characterized, often correlating with fluctuations in water quality parameters such as dissolved inorganic nitrogen and organic loading (Fang et al, 2023; Huang et al, 2024a; Li et al, 2024b). Further research has revealed structural and functional divergence between particle-associated (PA) and free-living (FL) bacteria, with suspended particles enriched in nitrifying, denitrifying, and organic-degrading bacteria, underscoring the critical role of particle-associated niches in driving nitrogen cycling (Huang et al, 2025). Moreover, comparisons between high- and low-yield systems have shown that the concentration of suspended particles is significantly higher in high-yield greenhouse ponds, and that shrimp production is closely associated with the relative abundance and activity of key functional genera involved in

nitrification and denitrification (Huang et al, 2024b). Collectively, these findings underscore the critical role of microbial communities in nutrient removal and system stability in small-scale greenhouse aquaculture systems. However, existing research has primarily focused on temporal dynamics and local environmental influences, leaving fundamental questions unresolved: To what extent does the core microbiome maintain functional consistency across geographically distinct systems, and how do interactions among core taxa underpin the stability and efficiency of nutrient cycling? Addressing these knowledge gaps is essential for elucidating the ecological mechanisms that enable effective water purification and for developing targeted microbial management strategies applicable across diverse geographic settings.

To address these knowledge gaps, we employed an integrated approach combining 16S rRNA gene amplicon sequencing and metagenomic analysis to characterize microbial communities in small-scale greenhouse aquaculture systems from two geographically distinct regions in South China—Hepu, Guangxi and Xuwen, Guangdong. The specific objectives were to: (i) characterize the taxonomic and functional profiles of both particle-associated and free-living microbial communities across regions to evaluate structural and functional divergence or convergence; (ii) identify core microbiomes and reconstruct metagenome-assembled genomes (MAGs) to decipher genomic potential related to key nutrient cycling processes, especially carbon, nitrogen, and sulfur metabolism; and (iii) characterize microbial interspecies interactions to uncover cooperative mechanisms that support functional stability. These findings provide novel insights into the ecological mechanisms enabling efficient nutrient removal in this near-closed aquaculture systems, with significant implications for microbial management strategies aimed at enhancing sustainability and water quality regulation.

2. Materials and methods

2.1. Sample collection

Water samples were collected in May 2023 from *L. vannamei* aquaculture ponds under a small greenhouse model in two major shrimp farming regions in South China—Xuwen County, Guangdong Province and Hepu County, Guangxi Province. Each pond is stocked with 60,000 shrimp post-larvae. Commercial feed is provided three times daily, with an initial feeding rate of 2.5 kg per meal. Thereafter, the feeding rate is dynamically adjusted based on growth indicators such as body length and weight, as well as the feeding behavior of the shrimp. Sampling was conducted during two critical culture stages, namely the early-to-mid (EM) stage at approximately 30–40 days post-stocking and the mid-to-late (ML) stage around 60–70 days post-stocking. From each pond, a composite water sample was obtained by combining water collected from three sampling points to ensure representativeness. For each sample, 1 L of water was processed using an Imhoff cone to concentrate settleable and suspended solids. The suspended particles from the bottom of the cone were collected and centrifuged at 12,000 rpm for 1 min. The resulting pellet was retained as the particle-associated microbial sample. The upper aqueous layer from the Imhoff cone was then filtered through a 0.22 μm polycarbonate membrane to capture free-living microorganisms. All samples were transferred to 2 mL cryotubes, flash-frozen in liquid

nitrogen, and subsequently stored at -80°C until further processing. Each sample set consisted of four biological replicates, which were taken from four different ponds in the same farm.

Samples were systematically labeled based on location, stage, and fraction; for instance, free-living microbial samples from Xuwen were designated XW_EM_FL and XW_ML_FL, while particle-associated samples from the same site were labeled XW_EM_PA and XW_ML_PA. Corresponding samples from Hepu were named HP_EM_FL, HP_ML_FL, HP_EM_PA, and HP_ML_PA. Additionally, particle-associated samples from the mid-to-late stage were selected for metagenomic sequencing, with three biological replicates per group.

2.2. DNA extraction and 16S rRNA gene amplicon sequencing

Total microbial genomic DNA was extracted from all samples using the E.Z.N.A.® soil DNA Kit (Omega Bio-Tek, Norcross, GA, USA) following the manufacturer's instructions. DNA quality and concentration were assessed by 1.0% agarose gel electrophoresis and a NanoDrop 2000 spectrophotometer (Thermo Fisher Scientific, Waltham, MA, USA), followed by storage at -80°C until further processing. The hypervariable V3-V4 region of the bacterial 16S rRNA gene was amplified using the primers 338F (5'-ACTCCTACGGGAGGCAGCAG-3') and 806R (5'-GGACTACHVGGGTWTCTAAT-3') (Liu et al, 2016) with a T100 Thermal Cycler (BIO-RAD, Hercules, CA, USA). The PCR products were excised from 2% agarose gels, purified using a PCR Clean-Up Kit (Omega Bio-Tek, USA), and quantified using a Qubit 4.0 fluorometer (Thermo Fisher Scientific, USA). Purified amplicons were pooled in equimolar amounts and subjected to paired-end sequencing on an Illumina Nextseq2000 platform (Illumina, San Diego, CA, USA) by Majorbio Bio-Pharm Technology Co, Ltd. (Shanghai, China) following standard protocols.

Raw sequencing reads were processed with fastp (v0.19.6) (Chen et al, 2018) for quality control and adapter trimming, and assembled with FLASH (v1.2.7) (Magoč & Salzberg, 2011). The resulting high-quality sequences were clustered into operational taxonomic units (OTUs) at 97% similarity using UPARSE (v7.1) (Edgar, 2013; Stackebrandt & Goebel, 1994). Taxonomic classification of OTUs was performed with the RDP classifier (v2.11) (Wang et al, 2007) against the SILVA ribosomal RNA gene database (v138) applying a 70% confidence threshold, which facilitated community composition analysis across multiple taxonomic levels.

Alpha diversity of the microbial community, including richness (Chao1 index) and diversity (Shannon index), was estimated using Mothur (v.1.30.2). The β-nearest taxon index (βNTI) was calculated using R software. To evaluate the relative contributions of deterministic and stochastic processes in microbiome assembly, a null model with 999 randomizations was applied to quantify βNTI, which standardizes the difference between observed βMNTD and its mean expectation under the null model based on phylogenetic information (Zhou & Ning, 2017).

2.3. Metagenomic sequencing, assembly and binning

DNA extracts were fragmented to an average size of approximately 350 bp using a Covaris M220 instrument (Gene Company Limited, Hong Kong, China) for paired-end library construction. Sequencing libraries were constructed with the NEXTflex™ Rapid DNA-Seq Kit (Bioo Scientific, Austin, TX, USA) and subjected to metagenomic sequencing on the Illumina NovaSeq™ X Plus platform. Raw reads were processed with fastp (v0.20.0) (Chen et al, 2018) for adapter trimming and removal of low-quality sequences (length < 50 bp or average quality score < 20). Quality-filtered data were assembled with MEGAHIT (v1.1.2) (Li et al, 2015), and contigs with lengths ≥ 300 bp were retained for downstream analysis. Those contigs with lengths ≥ 1000 bp were subsequently selected for binning using MetaBAT (v2.12.1) (Kang et al, 2015). Bin sets from individual and co-assemblies were de-replicated using dRep (v1.0.12) with an average nucleotide identity threshold ≥ 95% to eliminate redundant bins and select the highest quality genomes. Finally, 101 non-redundant species-level MAGs exhibiting medium- to high-quality characteristics (completeness > 50%, contamination < 10%) were recovered after quality evaluation with CheckM (v1.0.12) (Parks et al, 2015).

2.4. Taxonomic and functional annotation

Taxonomic and functional annotation of metagenomic contigs was conducted based on a non-redundant gene set derived from the assembly. Amino acid sequences were aligned using Diamond (v2.0.13) (Buchfink et al, 2015) against the Kyoto Encyclopedia of Genes and Genomes (KEGG), the National Center for Biotechnology Information (NCBI) non-redundant protein (NR) database and the Carbohydrate-Active Enzymes (CAZy) database under BLASTP parameters with an e-value threshold of $1e^{-5}$. This allowed retrieval of both taxonomic identity and functional assignments for the recovered genes. Through this approach, insights into microbial community structure, including abundance and distribution, as well as functional characteristics such as gene content and metabolic potential were obtained from particle-associated samples during the late culture stage across both geographic regions.

For MAGs, taxonomic classification was conducted with GTDB-Tk (v2.3.0) (Chaumeil et al, 2020). The relative abundance of each MAG within samples was quantified using CoverM (v0.6.1) (Aroney et al, 2025) by mapping quality-controlled reads to the reconstructed genomes. Coding sequences within MAGs were predicted with Prodigal (v2.6.3) (Hyatt et al, 2010). Functional annotation of these genes was carried out by homology searches against several databases, including KEGG, COG, and CAZy, to infer metabolic capabilities and functional profiles of the microbial populations. Additionally, nitrogen metabolic pathways were reconstructed based on KEGG module completeness.

2.5. Core microbial taxa identification

Core microbial taxa were determined based on both prevalence and abundance from 16S rRNA gene amplicon sequencing data. Specifically, three criteria were applied to screen for core bacterial genera: (1) ubiquitous genera, present in > 80% of all samples; (2) overall abundant genera, with an average relative abundance > 0.1%; and (3) frequently abundant genera, whose relative abundance exceeds 1% in > 50% of samples (Zhao et al, 2025). This multi-criterion approach enables the robust detection of taxa that are

both widespread and abundant, thereby highlighting microorganisms that are likely to play pivotal roles in downstream functional analyses.

2.6. Co-occurrence network construction and analysis

Microbial co-occurrence networks were constructed based on species annotation results together with functional gene abundance profiles or MAG abundance data. Pairwise associations were inferred using Spearman's correlation, and only those with an absolute correlation coefficient greater than 0.8 ($|r| > 0.8$) and a Benjamini-Hochberg false discovery rate (FDR)-adjusted p-value < 0.05 were retained as significant (Ling et al, 2022; Noble, 2009). Topological properties of the networks were calculated with the igraph package in R (v4.3.1), and network visualization was generated using Gephi (v0.10.1) (Bastian et al, 2009). This analysis revealed potential interactions involving nitrogen and sulfur metabolism genes, as well as among core MAGs.

2.7. Statistical analyses

The Kruskal-Wallis H test was employed to assess differences in alpha diversity indices (Chao1 and Shannon) across sample groups. The Wilcoxon rank-sum test was used to compare particle-associated microbial communities at different stages. Spearman correlation analysis was performed to evaluate the relationships between nitrogen metabolism and sulfur metabolism genes, as well as the 55 high-frequency and high-abundance MAGs. Statistical significance was determined at a threshold of $p < 0.05$. All statistical analyses were performed in R (v4.3.1).

3. Results

3.1. Microbial diversity divergence across geographic regions and culture stages

The microbial communities in small-scale greenhouse aquaculture ponds of *L. vannamei* were characterized via 16S rRNA sequencing to assess variations across two geographic regions (Hepu, HP and Xuwen, XW) and two culture stages (early-to-mid, EM; mid-to-late, ML). First, OTU-level analysis revealed distinct differences between the two regions (Fig. 1a). At the same culture stage, the number of OTUs in both free-living and particle-associated communities was much higher in HP than in XW. Among all samples, 490 OTUs were shared (accounting for only 4.26% of the total), while unique OTUs accounted for 52.74%, indicating marked regional divergence in microbial community composition. Alpha diversity analysis further revealed significant regional differences in species richness. Both free-living and particle-associated communities from HP exhibited significantly higher Chao1 indices than those from XW ($p < 0.05$). Within each region, microbial richness in both fractions increased slightly from the EM to the ML stage (Fig. 1b). Similarly, the Shannon diversity index was significantly higher in HP than in XW ($p < 0.05$) and also increased modestly over time in both regions (Fig. 1c).

Non-metric multidimensional scaling (NMDS) ordination based on Bray-Curtis dissimilarity revealed clear separation between microbial communities from HP and XW (stress < 0.2), confirming significant regional divergence (Fig. 1d). Distinct clustering was also observed between free-living and particle-associated communities, while samples from the same niche but different culture stages showed weaker divergence, indicating that niche partitioning had a stronger influence on community structure than culture stage. These results demonstrate that both geographic variation and niche differentiation significantly shaped microbial community structure in small-scale greenhouse aquaculture systems of *L. vannamei*.

Taxonomic profiling at the phylum level revealed that microbial communities were predominantly composed of Proteobacteria, Actinobacteriota, Bacteroidota, Patescibacteria, Chloroflexi, Verrucomicrobiota, Firmicutes, unclassified_k__norank__d__Bacteria, Desulfobacterota, Planctomycetota, and Bdellovibrionota (Fig. 1e). Among these, Proteobacteria, Actinobacteriota, Bacteroidota, and Patescibacteria were the dominant phyla across nearly all samples. Significant regional variations in phylum composition were observed, with Bacteroidota exhibiting higher relative abundances in both free-living and particle-associated communities from XW compared to HP. Stage-dependent successional dynamics were also evident within each region. In HP, the relative abundance of Chloroflexi was significantly higher in the ML stage than in the EM stage in both free-living and particle-associated communities ($p < 0.05$), with particularly pronounced enrichment in the particle-associated fraction. In XW, the relative abundance of Actinobacteriota in free-living samples increased significantly from EM to ML ($p < 0.05$), while Patescibacteria in free-living samples decreased significantly during this transition ($p < 0.05$).

3.2. Spatiotemporal succession of dominant taxa and identification of core taxa

Analysis of the taxonomic composition at the family level (Fig. 2a) revealed that Rhodobacteraceae was the most abundant family across all culture stages (EM and ML) and niches (free-living and particle-associated) in both regions, with relative abundances ranging from 12.8% to 50.6%, underscoring its fundamental ecological role in these aquaculture systems. Flavobacteriaceae also maintained high relative abundances in most samples. Notably, both Rhodobacteraceae and Flavobacteriaceae generally exhibited higher relative abundances in the XW region. In contrast, the family norank_o__PeM15 was more abundant in the HP region and exhibited a pronounced preference for the free-living niche during both culture stages. Its highest relative abundance (13.6% to 21.4%) was observed in the free-living fraction in the EM stage in HP, whereas in XW, it was only notably detected in free-living communities in the same EM stage. Saccharimonadaceae was relatively abundant in HP in both free-living and particle-associated communities, while in XW, it was primarily detected in the ML stage, especially in free-living communities. Demequinaceae was consistently enriched in particle-associated communities in the XW region during both EM and ML stages, indicating a clear niche preference; however, its abundance remained low across all samples from the HP region. Several other families displayed distinct niche-

specific distribution patterns. For example, Propionibacteriaceae and Intrasporangiaceae were consistently more abundant in particle-associated communities across different stages and regions, whereas Microbacteriaceae showed a clear preference for the free-living niche.

At the genus level (Fig. 2b), clear regional differentiation was observed among genera within the dominant family *Rhodobacteraceae*. Specifically, *Ruegeria* was persistently dominant in the XW region, with relative abundances ranging from 10.3% to 36.5%, significantly exceeding its abundances in the HP region (consistently below 8%), highlighting its region-specific importance. In contrast, *Donghicola* and *Marivita* were more abundant in the HP region. Notably, *unclassified_f__Rhodobacteraceae* was consistently present across all niches and culture stages in both regions, with relative abundances ranging from 4.5% to 18.8% in HP and from 3.7% to 21.0% in XW, emphasizing its role as a core and stable member of the microbiome. The genus *norank_f__norank_o__PeM15* followed the distribution pattern observed at the family level, showing a clear preference for the free-living niche in the HP region. Similarly, the distribution of *Demequina* aligned with that of its family, Demequinaceae, displaying consistent enrichment in particle-associated communities within the XW region. The genus *Robiginitalea* (affiliated with *Flavobacteriaceae*) was more enriched in the XW region, similar to the pattern of *Ruegeria*, while *unclassified_f__Saccharimonadaceae* preferentially occurred in the HP region. A notable divergence in niche preference was further observed at the genus level. In contrast to *norank_f__Propionibacteriaceae* and *norank_f__Intrasporangiaceae*, which were more abundant in particle-associated communities, *Candidatus Aquiluna* and *norank_f__norank_o__Candidatus Kaiserbacteria* preferentially colonized the free-living niche.

Based on established criteria (average relative abundance > 0.1%, occurrence in > 80% of all samples, and relative abundance > 1% in > 50% of samples), we identified the core microbial genera from two distinct regions. Among these, 113 genera exhibited an average relative abundance exceeding 0.1%, 204 genera were present in more than 80% of the samples, and 12 genera showed a relative abundance above 1% in over 50% of the samples (Table S1). A total of 12 core genera were identified, including *Ruegeria*, *unclassified_f__Rhodobacteraceae*, *norank_f__norank_o__PeM15*, *Demequina*, *Robiginitalea*, *norank_f__norank_o__Saccharimonadales*, *norank_f__Propionibacteriaceae*, *norank_f__Caldilineaceae*, *unclassified_f__Saprospiraceae*, *Tropicimonas*, *norank_f__Saccharimonadaceae*, and *unclassified_f__Saccharimonadaceae* (Fig. 2c).

3.3. Shifts in ecological processes governing microbial community assembly

To elucidate the ecological processes governing microbial community assembly, we assessed phylogenetic turnover using the βNTI. The overall βNTI values ranged from − 5.49 to 3.38 (Table S2), encompassing both stochastic (|βNTI| < 2) and deterministic (|βNTI| > 2) processes. A general decline in βNTI was observed from the EM to the ML stages in both the XW and HP regions (Fig. 3a). During the EM stage, most βNTI values for both particle-associated and free-living communities fell within the range of -2 and 2, reflecting the dominance of stochastic processes. As the system progressed to the ML

stage, βNTI values decreased noticeably, with many falling below − 2, especially among particle-associated communities, indicating a shift toward deterministic processes.

We further quantified the relative importance of different ecological processes (Fig. 3b). In particle-associated communities, stochastic processes dominated during the EM stage in both regions. This was particularly evident in HP, where community assembly was entirely governed by drift (and others) (100%), while in XW, stochastic processes also prevailed, represented by homogeneous dispersal (37.5%) and drift (and others) (25%). A clear transition occurred in the ML stage, as both regions shifted to deterministic-dominated assembly, with homogeneous selection contributing an identical, substantial proportion (62.5%) in particle-associated communities. Free-living communities exhibited less temporal variation. Stochastic processes, primarily drift (and others), predominated during the EM stage in both HP (75%) and XW (62.5%). By the ML stage, free-living communities in HP showed balanced deterministic (50% homogeneous selection) and stochastic influences (25% drift and others, 25% dispersal limitation), whereas those in XW remained largely stochastic, with drift (and others) accounting for 75% of the assembly processes. Collectively, these results demonstrate a temporal shift in microbial community assembly in small-scale greenhouse aquaculture ponds of *L. vannamei*, from predominantly stochastic processes in the EM stage to increasingly deterministic processes in the ML stage, with homogeneous selection playing a particularly prominent role in particle-associated communities.

To identify specific microbial taxa potentially associated with the observed assembly shifts, we examined differentially abundant genera in particle-associated communities between the EM and ML stages. A total of 102 and 39 genera showed significant changes in abundance ($p < 0.05$) between the different stages in the HP and XW regions, respectively (Table S3). The top 10 most differentially abundant genera between stages were identified, highlighting those that were significantly enriched from the EM to the ML stages (Fig. 3c). Specifically, in HP_ML_PA samples, significant enrichment was observed for *norank_f__Intrasporangiaceae*, *norank_f__AKYG1722*, *norank_f__JG30-KF-CM45*, *norank_f__norank_o__Actinomarinales*, *Xanthomarina*, and *Hanstruepera* ($p < 0.05$). In XW_ML_PA samples, taxa such as *norank_f__Steroidobacteraceae*, *TM7a*, *norank_f__JG30-KF-CM45*, *Woeseia*, *norank_f__norank_o__Candidatus_Kaiserbacteria*, and *Nitrosomonas* were significantly enriched ($p < 0.05$).

3.4. Metabolic functional profiles of particle-associated microbial communities

We performed metagenomic sequencing on particle-associated samples in the ML stage from both regions to profile the functional outcomes of their deterministic assembly. KEGG annotation revealed high functional consistency between regions at pathway level 3, with 459 of 465 annotated pathways shared between HP and XW (Fig. 4a). Notably, the top 10 most enriched pathways were fully consistent between the two regions, including Metabolic pathways, Biosynthesis of secondary metabolites, Microbial metabolism in diverse environments, Biosynthesis of cofactors, Carbon metabolism, Biosynthesis of amino acids, Quorum sensing, Two-component system, ABC transporters, and Purine

metabolism (Table S4). Functional annotation identified 9,957 genes associated with these pathways, with 8,752 genes (87.90%) shared between regions (Table S5).

Analysis of key metabolic pathways involved in the biogeochemical cycle revealed that genes associated with carbon metabolism were primarily linked to the reductive citrate cycle (Arnon-Buchanan cycle), the dicarboxylate-hydroxybutyrate cycle, the citrate cycle (TCA cycle), methanogenesis, and the 3-hydroxypropionate bi-cycle. Nitrogen metabolism was dominated by denitrification and dissimilatory nitrate reduction pathways, while sulfur metabolism primarily involved assimilatory sulfate reduction and thiosulfate oxidation by SOX complex (Fig. 4b). A network constructed from genes related to carbon, nitrogen, and sulfur metabolism contained 322 nodes and 7,712 edges, yielding a modularity index of 0.387. This relatively low modularity indicates that the network is weakly compartmentalized, with extensive cross-talk among the three metabolic pathways (Fig. 4c). In contrast, the network limited to nitrogen- and sulfur-related genes comprised 102 nodes and 798 edges and exhibited a higher modularity index of 0.464, indicating a more distinct modular organization and tighter functional interactions within modules (Fig. 4d).

To evaluate the organic matter degradation potential of particle-associated communities, we profiled the diversity and abundance of genes encoding CAZymes. The CAZymes identified in these communities fell into six major classes: glycoside hydrolases (GH), carbohydrate binding modules (CBM), auxiliary activities (AA), glycosyl transferases (GT), carbohydrate esterases (CE), and polysaccharide lyases (PL) (Fig. 4e). Among them, GHs were the most abundant CAZyme family in both regions and were significantly enriched compared with other categories. Taxonomic distribution analysis revealed that 89.14% of these CAZymes were affiliated with ten phyla, with Pseudomonadota, Actinomycetota, Bacteroidota, Chloroflexota, Planctomycetota dominating the community. At the genus level, these enzymes were predominantly associated with taxa such as *Caldilinea*, *Ilumatobacter*, *Candidatus_Promineifilum*, *Anaerolinea*, *Demequina*, *unclassified Candidatus_Saccharibacteria*, *Robiginitalea*, and *Ruegeria* (Fig. 4f).

We examined genes involved in the key nitrogen pathways of denitrification and dissimilatory nitrate reduction to assess the nitrogen metabolic potential of particle-associated microorganisms. Key genes included those for denitrification, including *nosZ* (K00376), *norB* (K04561), *nirS* (K15864), *napA* (K02567), *nirK* (K00368), *norC* (K02305), and *napB* (K02568), as well as for dissimilatory nitrate reduction, including *nrfA* (K03385), *nirB* (K00362), *nrfH* (K15876), and *nirD* (K00363) (Fig. 4e). These genes were predominantly distributed among several major phyla, including Pseudomonadota, Actinomycetota, Bacteroidota, and Chloroflexota. At the genus level, significant enrichment was observed within genera such as *Demequina*, *Caldilinea*, *Candidatus_Promineifilum*, *Ruegeria*, *Woeseia*, *Paracoccus*, and *Robiginitalea* (Fig. 4f).

The sulfur metabolism potential of particle-associated microbial communities was evaluated by analyzing genes involved in key sulfur metabolism pathways, including assimilatory sulfate reduction, thiosulfate oxidation by SOX complex. A total of 16 key genes were identified, comprising *soxZ* (K17227),

soxY (K17226), *soxX* (K17223), *soxD* (K22622), *soxC* (K17225), *soxB* (K17224), *soxA* (K17222), *sir* (K00392), *sat/met3* (K00958), *cysNC* (K00955), *cysN* (K00956), *cysJ* (K00380), *cysI* (K00381), *cysH* (K00390), *cysD* (K00957), and *cysC* (K00860) (Fig. 4e). These genes were mainly distributed across several phyla, including Pseudomonadota, Actinomycetota, Bacteroidota, Planctomycetota, and Chloroflexota, and were further enriched in genera such as *Ilumatobacter*, *Ruegeria*, *Robiginitalea*, *Demequina*, *Tetrasphaera*, *Paracoccus*, *Nitratireductor*, and *Marivita* (Fig. 4f). Notably, *Demequina*, *Robiginitalea*, and *Ruegeria* were established as the core bacterial genera in both the HP and XW regions (Fig. 2c). Their consistent presence, together with the enrichment of genes for CAZymes and those involved in nitrogen and sulfur metabolism (Fig. 4e), underscores their pivotal, multifunctional role in driving the biogeochemical cycling of organic carbon, nitrogen, and sulfur, thereby sustaining nutrient dynamics within these aquaculture systems.

3.5. Genomic traits and ecological interactions of core microbes from MAGs

Metagenome binning recovered 101 medium/high-quality MAGs spanning 9 phyla, dominated by Actinomycetota, Bacteroidota, Pseudomonadota, and Chloroflexota. These MAGs were assigned to 34 families, such as Flavobacteriaceae, Rhodobacteraceae, Saprospiraceae, Promineofilaceae, Dermatophilaceae, Demequinaceae, Ilumatobacteraceae, and Nitrosomonadaceae. A substantial proportion of these MAGs lacked complete taxonomic classification, with 95 (94.06%) unassigned at the species level and 34 (33.66%) at the genus level (Fig. 5a). A microbial co-occurrence network was constructed based on MAGs present in more than half of the samples, using a threshold of $|r| > 0.8$ and $p < 0.05$ ($n > 3$). The resulting network comprised 93 nodes and 670 edges, with a modularity index of 0.528 (Fig. 5b, Table 1). This indicates a moderately modular architecture reflecting distinct community modules within the particle-associated microbiome.

Table 1
Topological parameters of MAG-based co-occurrence network

Topological Parameter	**Value**
Average Degree	14.409
Network Diameter	7
Graph Density	0.157
Modularity	0.528
Average Clustering Coefficient	0.645
Average Path Length	2.984
Number of Nodes	93
Number of Edges	670

To identify the most prevalent and abundant lineages, we refined our focus to MAGs present in at least 5 samples and constituting the top 80% of total abundance in both regions, resulting in a set of 55 MAGs (Fig. 6a). These MAGs were primarily affiliated with the phyla Pseudomonadota, Bacteroidota, and Actinomycetota, distributed across 16 families including Flavobacteriaceae, Rhodobacteraceae, Saprospiraceae, Nitrosomonadaceae, Dermatophilaceae, Ilumatobacteraceae, and Cyclobacteriaceae. Among these 55 MAGs, 5 remained unclassified at the family level, 15 at the genus level, and 52 at the species level (Table S6).

KEGG pathway annotation of the 55 MAGs revealed that the top 20 enriched pathways were metabolic pathways, biosynthesis of secondary metabolites, microbial metabolism in diverse environments, biosynthesis of cofactors, biosynthesis of amino acids, carbon metabolism, two-component system, ABC transporters, quorum sensing, purine metabolism, pyruvate metabolism, oxidative phosphorylation, 2-oxocarboxylic acid metabolism, glycolysis/gluconeogenesis, ribosome, glyoxylate and dicarboxylate metabolism, glycine, serine and threonine metabolism, nucleotide metabolism, fatty acid metabolism, and biosynthesis of nucleotide sugars (Fig. 6b). We next performed a targeted functional analysis on eight representative MAGs from key taxa. These included MAGs from the core genera *Demequina* (MAG21, MAG64) and *Robiginitalea* (MAG10, MAG16), as defined in prior 16S rRNA analysis (Fig. 2c, Table S6), as well as *Nitrosomonas* (MAG22, MAG36, MAG39, MAG97), which showed marked enrichment in particle-associated communities in the ML stage (Fig. 3c, Table S6). The analysis focused on the top 20 pathways, as well as key nitrogen (denitrification, dissimilatory nitrate reduction) and sulfur (assimilatory sulfate reduction, thiosulfate oxidation by SOX complex) metabolism pathways. Analysis of the 50 most abundant genes from the top 20 pathways revealed their complete representation in all *Nitrosomonas* MAGs (MAG22, MAG36, MAG39, MAG97). The vast majority of these genes were also found in MAG10 and MAG16 (*Robiginitalea*), whereas a lower proportion (60% and 58%, respectively) were annotated in MAG64 and MAG21 (*Demequina*). The nitrite reductase gene *nirK* and the assimilatory sulfate reduction genes *cysD* and *cysN* were detected in all eight MAGs. Within the *Nitrosomonas* group, genes encoding nitric oxide reduction (*norB* and *norC*) and additional assimilatory sulfate reduction steps (*cysC*, *cysH*, and *cysI*) were almost universally present in all four MAGs (MAG22, MAG36, MAG39, MAG97). The presence of these denitrification genes is consistent with previous reports of concomitant nitrification and denitrification capacity in ammonia-oxidizing bacteria *Nitrosomonas* (Schmidt et al, 2004). In *Demequina*, the nitrate reductase genes *narG*, *narH*, and *narI* were present in MAG21, whereas MAG64 contained *narH* and *narI* together with some assimilatory sulfate reduction genes (*sat*, *sir*, and *cysH*). For *Robiginitalea*, both MAG10 and MAG16 contained the assimilatory sulfate reduction genes *cysC* and *cysH* (Fig. 6c).

Microbial interaction network analysis revealed associations between the eight core MAGs and other bacteria, identifying a total of 78 MAGs that were directly linked to them (Fig. 5b). With the exception of MAG16 and MAG39, which exhibited no significant interactions with others, all other core MAGs showed positive correlations in the network. Among these, MAG21, MAG64, MAG36, MAG22, and MAG97 were linked to the highest numbers of associated MAGs, at 18, 17, 16, 13, and 13, respectively (Table S7). Among the 18 MAGs correlated with MAG21, *unclassified_f__UBA6186*, *ZC4RG17*, *Demequina*, *UBA6265*,

and *unclassified_f__Competibacteraceae* displayed the strongest correlations (r > 0.9). Within the 17 MAGs related to MAG64, *unclassified_f__UBA6186*, *ZC4RG17*, *UBA6265*, and *unclassified_f__Competibacteraceae* were the most strongly correlated (r > 0.9). For MAG36, *JABDLO01* showed the highest correlation among its 16 associated MAGs (r > 0.9). Of the 13 MAGs linked to MAG22, *SZUA-117*, *unclassified_o__Jiangellales*, *Arenibacterium*, *Luteolibacter*, and *Nitrosomonas* had the highest correlations (r > 0.9). Regarding MAG97, *SZUA-117*, *Robiginitalea*, and *unclassified_f__UBA918* exhibited the strongest correlations among its 13 associated MAGs (r > 0.9) (Table 2).

Table 2
A list of bacterial taxa showing strong positive correlations (r > 0.9) with the core genera in the network analysis based on MAGs

Core MAG	Correlated MAG	Genus	Correlation (r)
MAG21 (*Demequina*)	MAG4	*unclassified_f__UBA6186*	0.941124
	MAG49	*ZC4RG17*	0.941124
	MAG54	*ZC4RG17*	0.941124
	MAG64	*Demequina*	1
	MAG82	*UBA6265*	0.941124
	MAG91	*unclassified_f__Competibacteraceae*	0.941124
MAG22 (*Nitrosomonas*)	MAG15	*SZUA-117*	0.985611
	MAG2	*unclassified_o__Jiangellales*	0.942857
	MAG20	*Arenibacterium_*	0.942857
	MAG33	*Luteolibacter*	0.941124
	MAG97	*Nitrosomonas*	0.942857
MAG36 (*Nitrosomonas*)	MAG59	*JABDLO01*	0.942857
MAG64 (*Demequina*)	MAG4	*unclassified_f__UBA6186*	0.941124
	MAG49	*ZC4RG17*	0.941124
	MAG54	*ZC4RG17*	0.941124
	MAG82	*UBA6265*	0.941124
	MAG91	*unclassified_f__Competibacteraceae*	0.941124
MAG97 (*Nitrosomonas*)	MAG15	*SZUA-117*	0.927634
	MAG37	*Robiginitalea*	0.941124
	MAG43	*Robiginitalea*	0.941124
	MAG44	*unclassified_f__UBA918*	0.941124
	MAG73	*Robiginitalea*	0.941124

Collectively, these interactions involve 22 MAGs spanning 13 genera, namely *Arenibacterium*, *Demequina*, *JABDLO01*, *Luteolibacter*, *Nitrosomonas*, *Robiginitalea*, *SZUA-117*, *UBA6265*, *unclassified_f__Competibacteraceae*, *unclassified_f__UBA6186*, *unclassified_f__UBA918*, *unclassified_o__Jiangellales*, and *ZC4RG17*. Given the importance of nitrogen metabolism in the small-

scale greenhouse aquaculture system, we further analyzed the nitrogen metabolic potential of both the eight core MAGs and the 22 strongly correlated MAGs. The eight core MAGs were enriched in genes related to denitrification and dissimilatory nitrate reduction to ammonium (DNRA), though pathways were incomplete due to the absence of *napA*, *napB*, and *nosZ*. However, combined annotation of all 22 MAGs revealed a complete set of genes necessary for both denitrification and DNRA (Fig. 6d). It is thus proposed that the eight core MAGs form metabolic alliances with a network of associated taxa (notably the 22 MAGs described) to form the functional core of the microbiome, which collaboratively reduces inorganic nitrogen levels in aquaculture water through coordinated denitrification and DNRA processes.

4. Discussion

The small-scale greenhouse farming model for Pacific white shrimp represents a transformative innovation in Chinese aquaculture, achieving high productivity and efficient utilization of water and land resources through its near-closed system design (Wan *et al*, 2017; Luo et al, 2021). However, the microbial mechanisms that sustain water quality in this system, especially across different geographic regions, remain insufficiently understood. In this study, microbial communities from two distinct production regions, HP (Hepu in Guangxi) and XW (Xuwen in Guangdong), exhibited significant taxonomic divergence. This was evidenced by a low proportion of shared OTUs, marked disparities in alpha diversity indices, and clear separation in NMDS ordination (Fig. 1a-d). The divergence likely stems from the cumulative effects of region-specific environmental filters, such as variations in source water geochemistry, sediment composition, and localized differences in agricultural practices (e.g, feed and probiotic use) (Hou et al, 2017; Huang et al, 2021; Debnath et al, 2025). The significantly higher species richness (Chao1) and diversity (Shannon) observed in HP suggest potentially more heterogeneous environmental conditions or differing nutrient inputs that support a broader microbial consortium (Nguyen et al, 2020; Miller and Allesina, 2023).

This geographic divergence is further reflected in the differential abundance of key taxa. For instance, the significantly higher relative abundance of Bacteroidota in XW (Fig. 1e) likely corresponds to their crucial role as primary degraders of complex organic wastes, such as residual feed and metabolic byproducts, which are characteristic of aquaculture environments (Fernández-Gómez et al, 2013; Rajeev et al, 2024). Moreover, within the keystone family Rhodobacteraceae, which exhibited consistent dominance across all regions, culture stages, and niches (12.8%–50.6% relative abundance; Fig. 2a), clear regional disparity was observed. Specifically, *Ruegeria* exhibited dominance in XW, while *Donghicola* and *Marivita* were more prevalent in HP (Fig. 2b). Members of Rhodobacteraceae are metabolically versatile, engaging in key processes such as organic matter degradation, nitrogen removal, sulfur oxidation, and the production of bioactive compounds, thereby making them indispensable for maintaining system stability (Pohlner et al, 2019). This regional substructure suggests that localized environmental factors may select for specific phylogenetic lineages from within this broadly adapted, functionally conserved group.

Despite the significant divergence in microbial community structures across geographically distinct small-scale greenhouse shrimp aquaculture systems, the microbial assembly processes in both regions exhibit a consistent temporal shift from stochastic dominance in the early-to-mid (EM) culture stage to deterministic control by the mid-to-late (ML) stage (Fig. 3a). This successional pattern mirrors ecological dynamics observed in engineered microbial systems, where initial colonization is largely governed by random dispersal and ecological drift, while mature communities are shaped by persistent environmental filtering (Dini-Andreote et al, 2015; Veach et al, 2016; Yu et al, 2021). During the EM stage, high resource availability from initial feeding and fluctuating environmental parameters (e.g, variable ammonia levels) likely attenuate selective pressures, enabling stochastic processes to prevail. As the culture progresses, the cumulative loading of organic waste and metabolic byproducts (e.g, nitrite) establishes a strong and consistent selective environment, favoring taxa with specialized metabolic pathways for nutrient transformation and thereby driving the transition to deterministic assembly (Zheng et al, 2024). Notably, this assembly shift was more pronounced in particle-associated communities, where homogeneous selection accounted for 62.5% of assembly processes in both regions during the ML stage (Fig. 3b). This cross-regional consistency suggests that the selective pressures inherent to the near-closed shrimp aquaculture system, such as minimal water exchange, high C/N ratios, and particle-rich microenvironments, are sufficiently potent to override regional heterogeneities, thereby favoring functionally convergent taxa irrespective of geographic origin (Guo et al, 2022).

Deterministic selection is pivotal for ensuring the functional stability of microbial communities (Zhang et al, 2022). This principle aligns with the concept of functional redundancy, wherein phylogenetically distinct taxa within an ecosystem can perform equivalent core ecological functions (Louca et al, 2018). Under consistent environmental pressures, deterministic processes preferentially filter for specific functional traits rather than particular taxonomic groups, leading to alternative community compositions with similar functional outputs (Song et al, 2022). Our observations support this notion; despite the presence of distinct particle-associated microbial community structures between the HP and XW regions, metagenomic analysis revealed a high degree of functional convergence in their ML-stage microbiomes. Notably, 459 out of 465 annotated KEGG pathways were shared between the two regions (Fig. 4a). The near-complete overlap of these pathways, particularly those associated with key nitrogen and sulfur transformation processes (Fig. 4b), demonstrates that the system deterministically selects for a conserved suite of biochemical functions essential for its ecological maintenance and stability.

The small-scale greenhouse aquaculture systems exhibited a high potential for organic matter degradation, as evidenced by the high relative abundance of CAZymes, with glycoside hydrolases (GHs) being particularly dominant (Fig. 4e). The majority of these CAZymes were affiliated with bacterial phyla such as Pseudomonadota, Actinomycetota, and Bacteroidota (Fig. 4e), which are well-recognized as primary degraders of complex organic matter in aquaculture systems (Rajeev et al, 2024). In environments characterized by high organic loading, such as aquaculture systems, the degradation of organic matter provides labile carbon that likely serves as a source of carbon or electron donors essential for driving energy-intensive nitrogen and sulfur transformation processes (Robinson et al, 2018). Such close coupling between carbon, nitrogen, and sulfur cycling is reflected in the relatively low

modularity (0.387) of the co-occurrence network constructed from genes involved in these three metabolic pathways (Fig. 4c), indicating extensive functional cross-talk and integrated processing. However, the subnetwork specifically linking nitrogen and sulfur cycling genes displayed a higher degree of modularity (0.464; Fig. 4d), suggesting more specialized and tightly regulated interactions within these two cycles. This pattern reflects a system-level optimization where a more modular N-S association enables dedicated and precise control over inorganic nitrogen removal and sulfur detoxification, whereas the tightly integrated C-N-S network supports holistic metabolic coupling and resource efficiency.

The reconstruction of 101 medium/high-quality MAGs and subsequent co-occurrence network analysis revealed a tightly interconnected microbial consortium (Fig. 5b). Interactions within this network were predominantly positive, suggesting prevalent mutualistic or commensal relationships, such as metabolite cross-feeding or shared niche preferences, which are known to enhance community stability and functional resilience (Butler and O'Dwyer, 2018; Kodera et al, 2022). The network centered on eight core MAGs (affiliated with *Demequina*, *Robiginitalea*, and *Nitrosomonas*), which were linked to 78 additional taxa. This network holds significant functional implications. While the eight core MAGs themselves harbored incomplete pathways for denitrification and DNRA (lacking genes such as *napA*, *napB*, and *nosZ*), the combined genomic potential of the core MAGs and their 22 strongly correlated partners encoded a complete gene set for these key nitrogen transformation processes (Fig. 6d). This demonstrates that critical inorganic nitrogen removal is not achieved by a single organism but emerges through functional complementarity within a tightly coupled consortium. Thus, although individual taxa may possess incomplete metabolic capacities, functional collaboration within microbial consortia enables the performance of entire, ecologically vital pathways (Yue et al, 2019; Zhang et al, 2023; Roothans et al, 2025). This functional collaboration provides a mechanistic explanation for the sustained high-efficiency nitrogen removal observed in this aquaculture model (Huang et al, 2024a). These insights have practical implications for managing microbial communities in aquaculture. Interventions aimed at fostering specific functional groups and their cooperative interactions may be more effective than those targeting specific taxonomic identities (Lorgen-Ritchie et al, 2023). The identified core MAGs and their cooperative partners provide a selection of candidate strains for developing synthetic microbial communities (SynComs), which could be deployed to enhance water purification efficiency. Overall, the findings highlight the potential of targeting core microbial consortia, rather than single-species inoculants, for probiotic development to improve nitrogen removal in the small-scale greenhouse aquaculture systems.

5. Conclusion

In summary, this study demonstrates that deterministic assembly processes in near-closed small-scale greenhouse aquaculture systems drive the formation of a functionally convergent and cooperative particle-associated core microbiome, despite taxonomic divergence across regions. The shift from stochastic to deterministic assembly, the central role of particle-associated niches, and the cooperative interactions among core taxa collectively sustain efficient nutrient cycling and water quality. These

findings advance fundamental understanding of microbial ecological dynamics in engineered aquaculture systems and establish a mechanistic basis for targeted microbiome manipulation strategies.

Abbreviations

EM
Early-to-mid
ML
Mid-to-late
DNRA
Dissimilatory nitrate reduction to ammonium
MAGs
Metagenome-assembled genomes
C/N
carbon-to-nitrogen
BFT
Biofloc technology
XW
Xuwen County, Guangdong Province
HP
Hepu County, Guangxi Province
PA
Particle-associated
FL
Free-living

Declarations

Ethics approval and consent to participate

Not applicable.

Consent for publication

Not applicable.

Competing interests

The authors declare that they have no competing interests.

Funding

This work was financially supported by the National Natural Science Foundation of China (32303063 and 32460930), the Hainan Provincial Natural Science Foundation of China (324MS022), the Innovational Fund for Scientific and Technological Personnel of Hainan Province (KJRC2023C40), and the Hainan Agricultural Production Research System (HNARS-10-G03).

Author Contribution

Ni Liu: Writing – original draft, Writing – review & editing, Visualization, Software, Methodology. Zhiyuan Yan: Writing – original draft, Methodology, Formal analysis, Data curation. Yuxing Xie: Writing – original draft, Methodology, Visualization. Hao Long: Supervision, Conceptualization. Xiaoni Cai: Supervision, Conceptualization. Aiyou Huang: Supervision, Conceptualization. Yanhua Zeng: Writing – original draft, Writing – review & editing, Supervision, Funding acquisition, Conceptualization. Zhenyu Xie: Writing – review & editing, Supervision, Funding acquisition, Conceptualization.

Acknowledgement

NL gratefully acknowledges classmates from the College of Marine Biology and Fisheries, Hainan University, who provided valuable support on samples collection in this experiment.

Data Availability

The raw 16S rRNA amplicon and metagenomic sequencing data have been deposited in the NCBI BioProject database under accession numbers PRJNA1331529 (https://www.ncbi.nlm.nih.gov/bioproject/?term=PRJNA1331529) and PRJNA1331465 (https://www.ncbi.nlm.nih.gov/bioproject/?term=PRJNA1331465), respectively.

References

1. Aroney STN, Newell RJP, Nissen JN, Camargo AP, Tyson GW, Woodcroft BJ. CoverM: read alignment statistics for metagenomics. Bioinformatics. 2025;41(4). https://doi.org/10.1093/bioinformatics/btaf147.
2. Bastian M, Heymann S, Jacomy M, Gephi. An open source software for exploring and manipulating networks. Proceedings of the International AAAI Conference on Web and Social Media. 2009; 3 (1), 361–362. https://doi.org/10.1609/icwsm.v3i1.13937
3. Buchfink B, Xie C, Huson DH. Fast and sensitive protein alignment using DIAMOND. Nat Methods. 2015;12(1):59–60. https://doi.org/10.1038/nmeth.3176.

4. Butler S, O'Dwyer JP. Stability criteria for complex microbial communities. Nat Commun. 2018;9(1):2970. https://doi.org/10.1038/s41467-018-05308-z.
5. Chang Z, Neori A, He Y, Li J, Qiao L, Preston SI, Liu P, Li J. Development and current state of seawater shrimp farming, with an emphasis on integrated multi-trophic pond aquaculture farms, in China – a review. Reviews Aquaculture. 2020;12(4):2544–58. https://doi.org/10.1111/raq.12457.
6. Chaumeil PA, Mussig AJ, Hugenholtz P, Parks DH. GTDB-Tk: a toolkit to classify genomes with the Genome Taxonomy Database. Bioinformatics. 2020;36(6):1925–7. https://doi.org/10.1093/bioinformatics/btz848.
7. Chen S, Zhou Y, Chen Y, Gu J. fastp: an ultra-fast all-in-one FASTQ preprocessor. Bioinformatics. 2018;34(17):i884–90. https://doi.org/10.1093/bioinformatics/bty560.
8. Chen Z, Li J, Zhai Q, Chang Z, Li J. Nitrogen cycling process and application in different prawn culture modes. Reviews Aquaculture. 2024;16(4):1580–602. https://doi.org/10.1111/raq.12912.
9. Debnath B, Sharma R, Balan B, Sultana T, Chowdhury MAH, Barman BK. Seasonal dynamics and factors shaping microbiomes in freshwater finfish earthen aquaculture ponds in Bangladesh. Environ Microbiome. 2025;20(1):42. https://doi.org/10.1186/s40793-025-00687-5.
10. Dini-Andreote F, Stegen JC, van Elsas JD, Salles JF. Disentangling mechanisms that mediate the balance between stochastic and deterministic processes in microbial succession. Proc Natl Acad Sci USA. 2015;112(11):E1326–32. https://doi.org/10.1073/pnas.1414261112.
11. Edgar RC. UPARSE: highly accurate OTU sequences from microbial amplicon reads. Nat Methods. 2013;10(10):996–8. https://doi.org/10.1038/nmeth.2604.
12. Emerenciano MGC, Miranda-Baeza A, Martínez-Porchas M, Poli MA, Vieira FN. Biofloc technology (BFT) in shrimp farming: Past and present shaping the future. Front Mar Sci. 2021;8. https://doi.org/10.3389/fmars.2021.813091.
13. Fang Y, Li H, Wang L, Wan X, Shi W, Yang Z, Jiang Q, Shen H, Hu R, Guan X, Yang J. Study on bacterial community structure in rearing water in small greenhouse of *Litopenaeus vannamei* (in Chinese). South China Fisheries Sci. 2023;19(3):29–41. https://doi.org/10.12131/20220205.
14. Fernández-Gómez B, Richter M, Schüler M, Pinhassi J, Acinas SG, González JM, Pedrós-Alió C. Ecology of marine Bacteroidetes: a comparative genomics approach. ISME J. 2013;7(5):1026–37. https://doi.org/10.1038/ismej.2012.169.
15. Fisheries bureau of the ministry of agriculture and rural affairs. 2024. China fishery statistical yearbook 2024.
16. Guo H, Dong P, Gao F, Du C, Fu J, Liu H, Gao P. Sucrose addition directionally enhances bacterial community convergence and network stability of the shrimp culture system. NPJ Biofilms Microbiomes. 2022;8(1):22. https://doi.org/10.1038/s41522-022-00288-x.
17. Hou D, Zhang P, Li Z, Zhang Q, Wang Y. Environmental factors shape water microbial community structure and function in shrimp cultural enclosure ecosystems. Front Microbiol. 2017;8:2359. https://doi.org/10.3389/fmicb.2017.02359.

18. Huang F, Zhang Y, Wang Y, Li A. Environmental water and sediment microbial communities shape intestine microbiota for host health: the central dogma in an anthropogenic aquaculture ecosystem. Front Microbiol. 2021;12:772149. https://doi.org/10.3389/fmicb.2021.772149.
19. Huang Y, Jiang K, Liu M, Wang B, Wang L. Microbial community dynamics and nitrogen transformation associated with turbid-turned culture stage of Pacific white shrimp, *Litopenaeus vannamei* in small greenhouse farms. Aquaculture. 2024a;593:741285. https://doi.org/10.1016/j.aquaculture.2024.741285.
20. Huang Y, Wang B, Liu M, Ren Z, Jiang K, Zhong C, Xu K, Gao Y, Wang L. Differences in water quality, bacterial structure and function of particle-associated bacteria and surrounding bacteria in small greenhouse farms of *Litopenaeus vannamei* under different yield levels. J Fish Sci China. 2024b;31(12):1484–96. https://doi.org/10.12264/JFSC2024-0190.
21. Huang Y, Liu M, Jiang K, Zhong C, Xu K, Wang B, Wang L. The dynamic features and microbial mechanism of nitrogen transformation in small greenhouse farming system of Pacific white shrimp, *Litopenaeus vannamei*. Aquaculture. 2025;605:742557. https://doi.org/10.1016/j.aquaculture.2025.742557.
22. Hyatt D, Chen GL, LoCascio PF, Land ML, Larimer FW, Hauser LJ. Prodigal: prokaryotic gene recognition and translation initiation site identification. BMC Bioinformatics. 2010;11(1):119. https://doi.org/10.1186/1471-2105-11-119.
23. Joyni MJ, Kurup BM, Avnimelech Y. Bioturbation as a possible means for increasing production and improving pond soil characteristics in shrimp-fish brackish water ponds. Aquaculture. 2011;318(3–4):464–70. https://doi.org/10.1016/j.aquaculture.2011.05.019.
24. Kang DD, Froula J, Egan R, Wang Z. MetaBAT, an efficient tool for accurately reconstructing single genomes from complex microbial communities. PeerJ. 2015;3:e1165. https://doi.org/10.7717/peerj.1165.
25. Kodera SM, Das P, Gilbert JA, Lutz HL. Conceptual strategies for characterizing interactions in microbial communities. IScience. 2022;25(2):103775. https://doi.org/10.1016/j.isci.2022.103775.
26. Li D, Liu CM, Luo R, Sadakane K, Lam TW. MEGAHIT: an ultra-fast single-node solution for large and complex metagenomics assembly via succinct *de Bruijn* graph. Bioinformatics. 2015;31(10):1674–6. https://doi.org/10.1093/bioinformatics/btv033.
27. Li E, Wang X, Chen K, Xu C, Qin JG, Chen L. Physiological change and nutritional requirement of Pacific white shrimp *Litopenaeus vannamei* at low salinity. Reviews Aquaculture. 2017;9(1):57–75. https://doi.org/10.1111/raq.12104.
28. Li H, Gu S, Wang L, Shi W, Jiang Q, Wan X. Dynamic changes of environment and gut microbial community of *Litopenaeus vannamei* in greenhouse farming and potential mechanism of gut microbial community construction. Fishes. 2024b;9(5):155. https://doi.org/10.3390/fishes9050155.
29. Li J, Zhu Z, Lv X, Hu X, Tan H, Liu W, Luo G. Exploring single-stage oxic process for simultaneous rapid recovery of phosphate and nitrate via bioflocs to promote circular economic. Chem Eng J. 2024a;497:154575. https://doi.org/10.1016/j.cej.2024.154575.

30. Ling N, Wang T, Kuzyakov Y. Rhizosphere bacteriome structure and functions. Nat Commun. 2022;13(1):836. https://doi.org/10.1038/s41467-022-28448-9.
31. Liu C, Zhao D, Ma W, Guo Y, Wang A, Wang Q, Lee DJ. Denitrifying sulfide removal process on high-salinity wastewaters in the presence of *Halomonas* sp. Appl Microbiol Biotechnol. 2016;100(3):1421–6. https://doi.org/10.1007/s00253-015-7039-6.
32. Lorgen-Ritchie M, Uren Webster T, McMurtrie J, Bass D, Tyler CR, Rowley A, Martin SAM. Microbiomes in the context of developing sustainable intensified aquaculture. Front Microbiol. 2023;14:1200997. https://doi.org/10.3389/fmicb.2023.1200997.
33. Louca S, Polz MF, Mazel F, Albright MBN, Huber JA, O'Connor MI, Ackermann M, Hahn AS, Srivastava DS, Crowe SA, Doebeli M, Parfrey LW. Function and functional redundancy in microbial systems. Nat Ecol Evol. 2018;2(6):936–43. https://doi.org/10.1038/s41559-018-0519-1.
34. Luo G, Ju R, Lu J, Wang H, Yu L. Application and exploration of small shed culture mode of *Litopenaeus vannamei*; in Rudong (in Chinese). Open J Fisheries Res. 2021;08(03):95–102. https://doi.org/10.12677/OJFR.2021.83011.
35. Magoč T, Salzberg SL. FLASH: fast length adjustment of short reads to improve genome assemblies. Bioinformatics. 2011;27(21):2957–63. https://doi.org/10.1093/bioinformatics/btr507.
36. Miller ZR, Allesina S. Habitat heterogeneity, environmental feedbacks, and species coexistence across timescales. Am Nat. 2023;202(2):E53–64. https://doi.org/10.1086/724821.
37. Nguyen J, Lara-Gutiérrez J, Stocker R. Environmental fluctuations and their effects on microbial communities, populations and individuals. FEMS Microbiol Rev. 2020;44(6):741–57. https://doi.org/10.1093/femsre/fuaa068.
38. Noble WS. How does multiple testing correction work? Nat Biotechnol. 2009;27(12):1135–7. https://doi.org/10.1038/nbt1209-1135.
39. Parks DH, Imelfort M, Skennerton CT, Hugenholtz P, Tyson GW. CheckM: assessing the quality of microbial genomes recovered from isolates, single cells, and metagenomes. Genome Res. 2015;25(7):1043–55. https://doi.org/10.1101/gr.186072.114.
40. Pohlner M, Dlugosch L, Wemheuer B, Mills H, Engelen B, Reese BK. The majority of active *Rhodobacteraceae* in marine sediments belong to uncultured genera: a molecular approach to link their distribution to environmental conditions. Front Microbiol. 2019;10:659. https://doi.org/10.3389/fmicb.2019.00659.
41. Rajeev M, Jung I, Kang I, Cho JC. Genome-centric metagenomics provides insights into the core microbial community and functional profiles of biofloc aquaculture. MSystems. 2024;9(10). https://doi.org/10.1128/msystems.00782-24.
42. Robinson G, Freitas D, Thomson B, Kutti T. Carbon amendment stimulates benthic nitrogen cycling during the bioremediation of particulate aquaculture waste. Biogeosciences. 2018;15(6):1863–75. https://doi.org/10.5194/bg-15-1863-2018.
43. Roothans N, van Loosdrecht MCM, Laureni M. Metabolic labour division trade-offs in denitrifying microbiomes. ISME J. 2025;19(1). https://doi.org/10.1093/ismejo/wraf020.

44. Schmidt I, van Spanning RJ, Jetten MS. Denitrification and ammonia oxidation by *Nitrosomonas europaea* wild-type, and *NirK*- and *NorB*-deficient mutants. Microbiol (Reading). 2004;150(12):4107–14. https://doi.org/10.1099/mic.0.27382-0.
45. Song W, Liu J, Qin W, Huang J, Yu X, Xu M, Stahl D, Jiao N, Zhou J, Tu Q. Functional traits resolve mechanisms governing the assembly and distribution of nitrogen-cycling microbial communities in the global ocean. mBio. 2022;13(2). https://doi.org/10.1128/mbio.03832-21.
46. Stackebrandt E, Goebel BM. Taxonomic note: a place for DNA-DNA reassociation and 16S rRNA sequence analysis in the present species definition in bacteriology. Int J Syst Evol MicroBiol. 1994;44(4):846–9. https://doi.org/10.1099/00207713-44-4-846.
47. Veach AM, Stegen JC, Brown SP, Dodds WK, Jumpponen A. Spatial and successional dynamics of microbial biofilm communities in a grassland stream ecosystem. Mol Ecol. 2016;25(18):4674–88. https://doi.org/10.1111/mec.13784.
48. Wan X. *Litopenaeus vannamei* 'Rudong small shed' mode of development status analysis (in Chinese). Sci Fish Farming. 2017. https://doi.org/10.14184/j.cnki.issn1004-843x.2017.04.001.
49. Wang Q, Garrity GM, Tiedje JM, Cole JR. Naïve Bayesian classifier for rapid assignment of rRNA sequences into the new bacterial taxonomy. Appl Environ Microbiol. 2007;73(16):5261–7. https://doi.org/10.1128/AEM.00062-07.
50. Wani SM, Chesti A, Rehman S, Chandra Nautiyal V, Bhat IA, Ahmad I. Repurposing and reusing aquaculture wastes through a biosecure microfloc technology. Environ Res. 2025;274:121214. https://doi.org/10.1016/j.envres.2025.121214.
51. Yu J, Tang SN, Lee PKH. Microbial communities in full-scale wastewater treatment systems exhibit deterministic assembly processes and functional dependency over time. Environ Sci Technol. 2021;55(8):5312–23. https://doi.org/10.1021/acs.est.0c06732.
52. Yu YB, Lee JH, Choi JH, Choi YJ, Jo AH, Choi CY, Kang JC, Kim JH. The application and future of biofloc technology (BFT) in aquaculture industry: A review. J Environ Manage. 2023;342:118237. https://doi.org/10.1016/j.jenvman.2023.118237.
53. Yue H, Zhang Y, He Y, Wei G, Shu D. Keystone taxa regulate microbial assemblage patterns and functional traits of different microbial aggregates in simultaneous anammox and denitrification (SAD) systems. Bioresour Technol. 2019;290:121778. https://doi.org/10.1016/j.biortech.2019.121778.
54. Zheng X, Hou D, Huang Z, He Z, He J, Yan Q. Microeukaryotic community dynamics and assembly mechanisms in shrimp aquaculture ponds. Aquaculture. 2024;590(000):741091. https://doi.org/10.1016/j.aquaculture.2024.741091.
55. Zhang IH, Sun X, Jayakumar A, Fortin SG, Ward BB, Babbin AR. Partitioning of the denitrification pathway and other nitrite metabolisms within global oxygen deficient zones. ISME Commun. 2023;3(1). https://doi.org/10.1038/s43705-023-00284-y.
56. Zhang L, Gong X, Xu R, Guo K, Wang L, Zhou Y. Responses of mesophilic anaerobic sludge microbiota to thermophilic conditions: Implications for start-up and operation of thermophilic THP-

AD systems. Water Res. 2022;216:118332. https://doi.org/10.1016/j.watres.2022.118332.

57. Zhao Y, Hu J, Wang J, Yao X, Zhang T, Hu B. Comammox *Nitrospira* act as key bacteria in weakly acidic soil via potential cobalamin sharing. iMeta. 2025;4(1). https://doi.org/10.1002/imt2.271.

58. Zhou J, Ning D. Stochastic community assembly: Does it matter in microbial ecology? Microbiol Mol Biol Rev. 2017;81(4). https://doi.org/10.1128/MMBR.00002-17.

59. Zhu W, Yuan G, Song Z, Li Q, Liu C, Xu A, Luan Y, Liu Y. In situ biofilm aquaculture systems (in situ BFSs) for *Litopenaeus vannamei*: A review. Reviews Aquaculture. 2025;17(4). https://doi.org/10.1111/raq.70058.

Figures

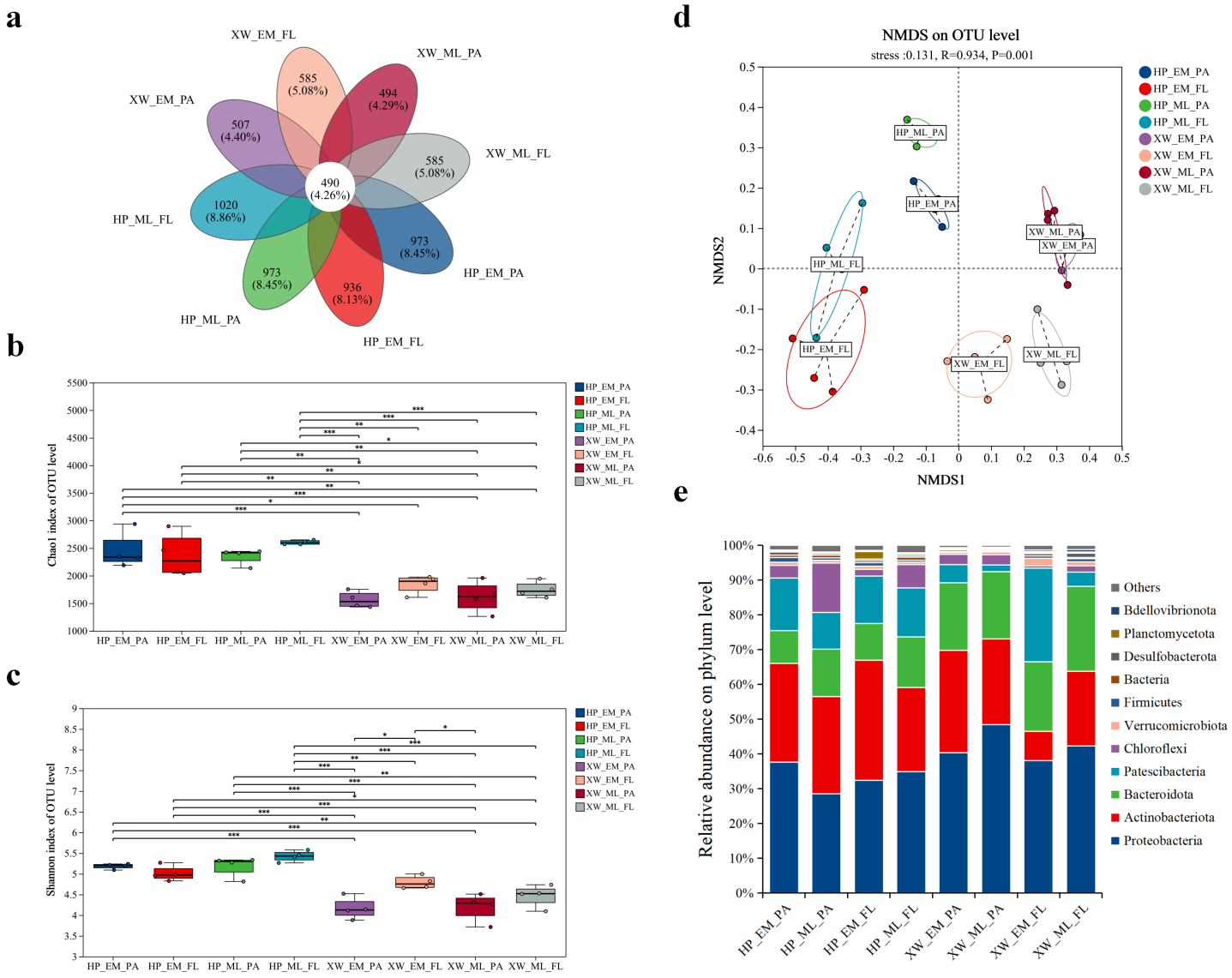

Figure 1

Microbial community dynamics of free-living and particle-associated bacteria in small-scale greenhouse aquaculture ponds of *L. vannamei* across different geographic regions and culture stages. (a) Venn diagram of shared and unique OTUs among experimental groups. (b) Alpha diversity (Chao1 index). (c) Chao1 index (Shannon index). (d) NMDS ordination based on Bray-Curtis dissimilarity. (e) Relative abundance of microbial taxa at the phylum level.

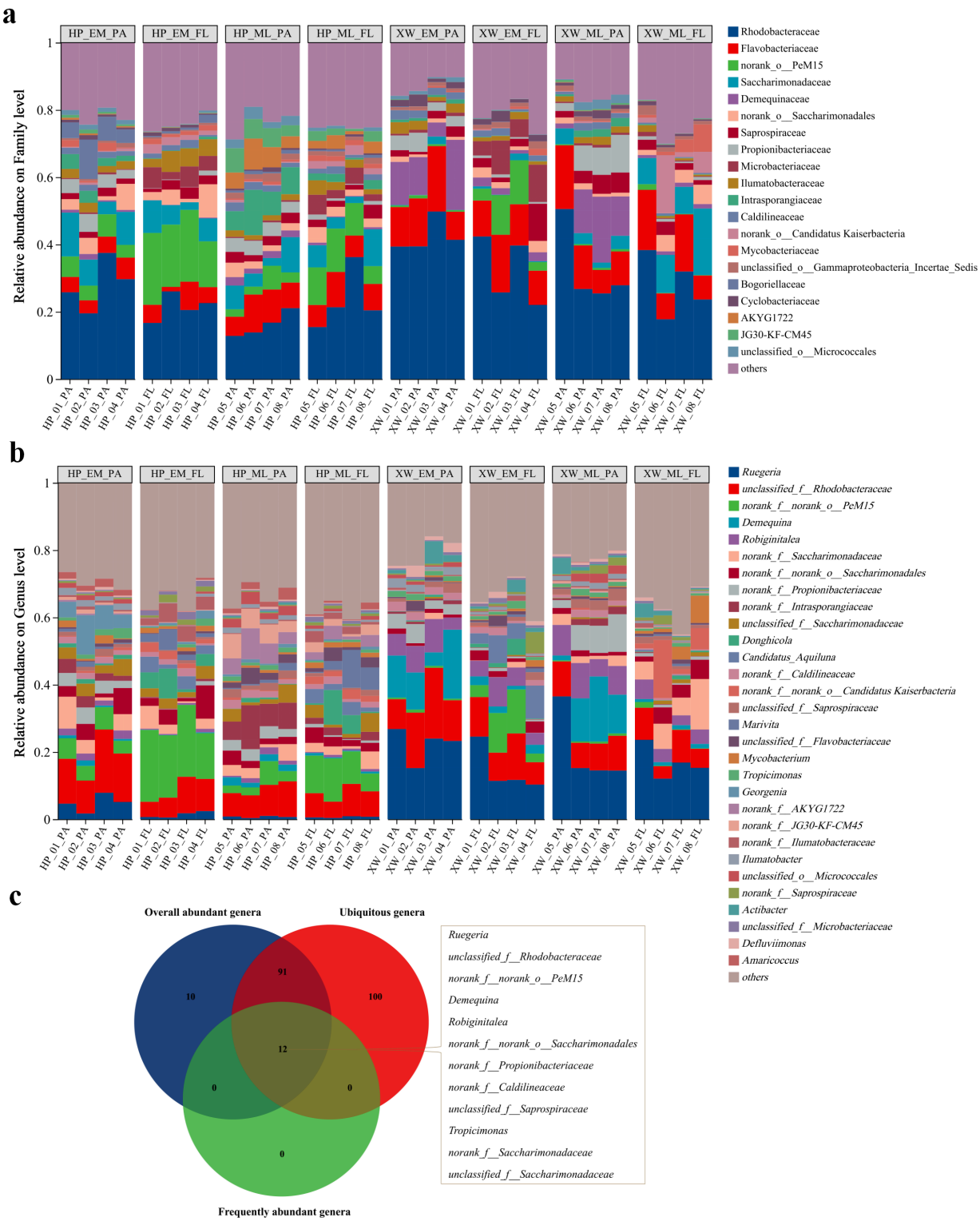

Figure 2

Microbial composition of free-living and particle-associated bacteria in small-scale greenhouse aquaculture ponds of *L. vannamei* across different geographic regions and culture stages. (a) Relative abundance at the family level. (b) Relative abundance at the genus level. (c) Venn diagram showing the selection of core microbial taxa.

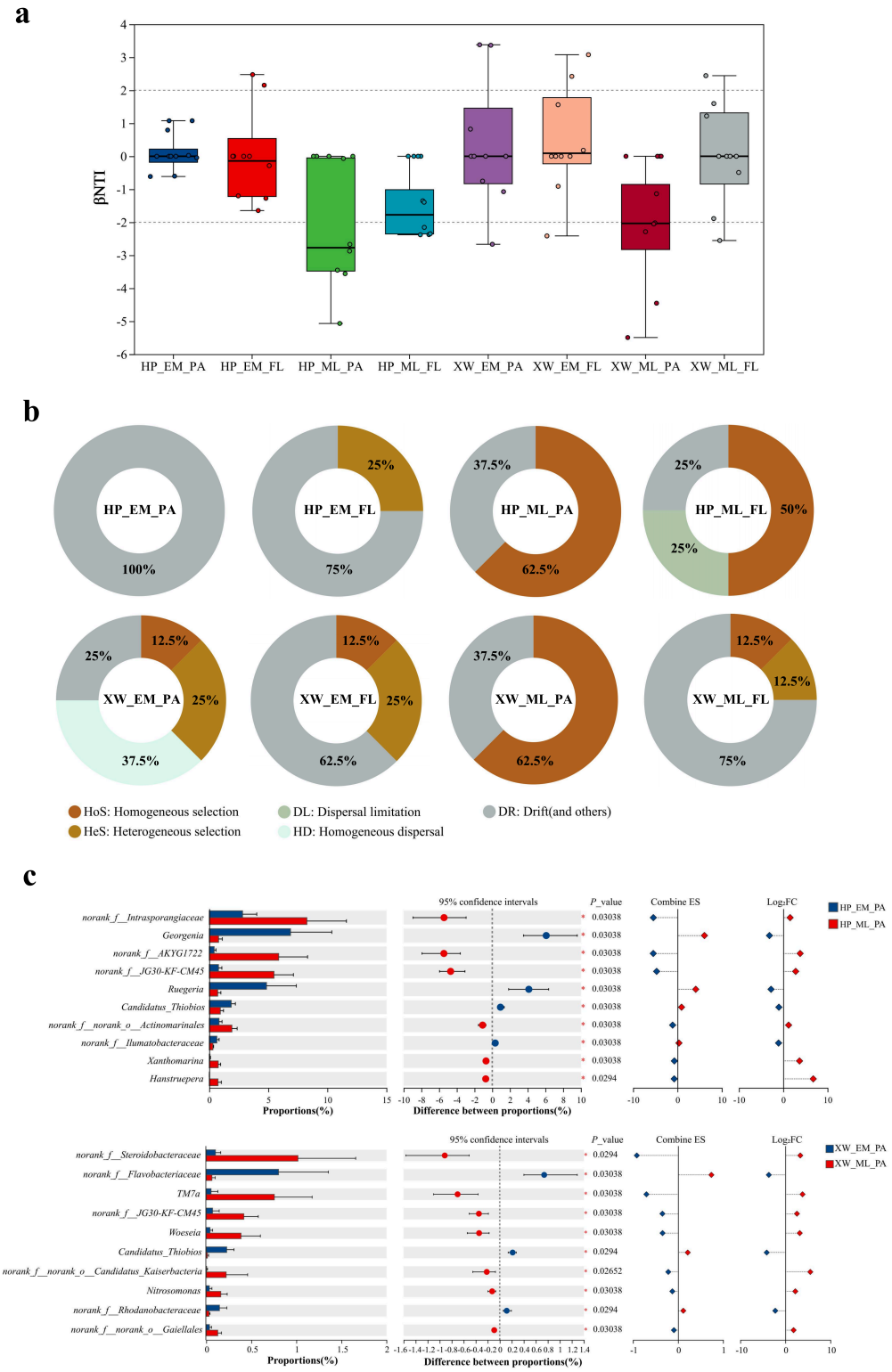

Figure 3

Microbial community assembly processes in small-scale greenhouse aquaculture ponds of *L. vannamei*. (a) Box plot of βNTI values. (b) Relative contribution of different ecological processes. (c) Genus-level differences between groups (Wilcoxon rank-sum test).

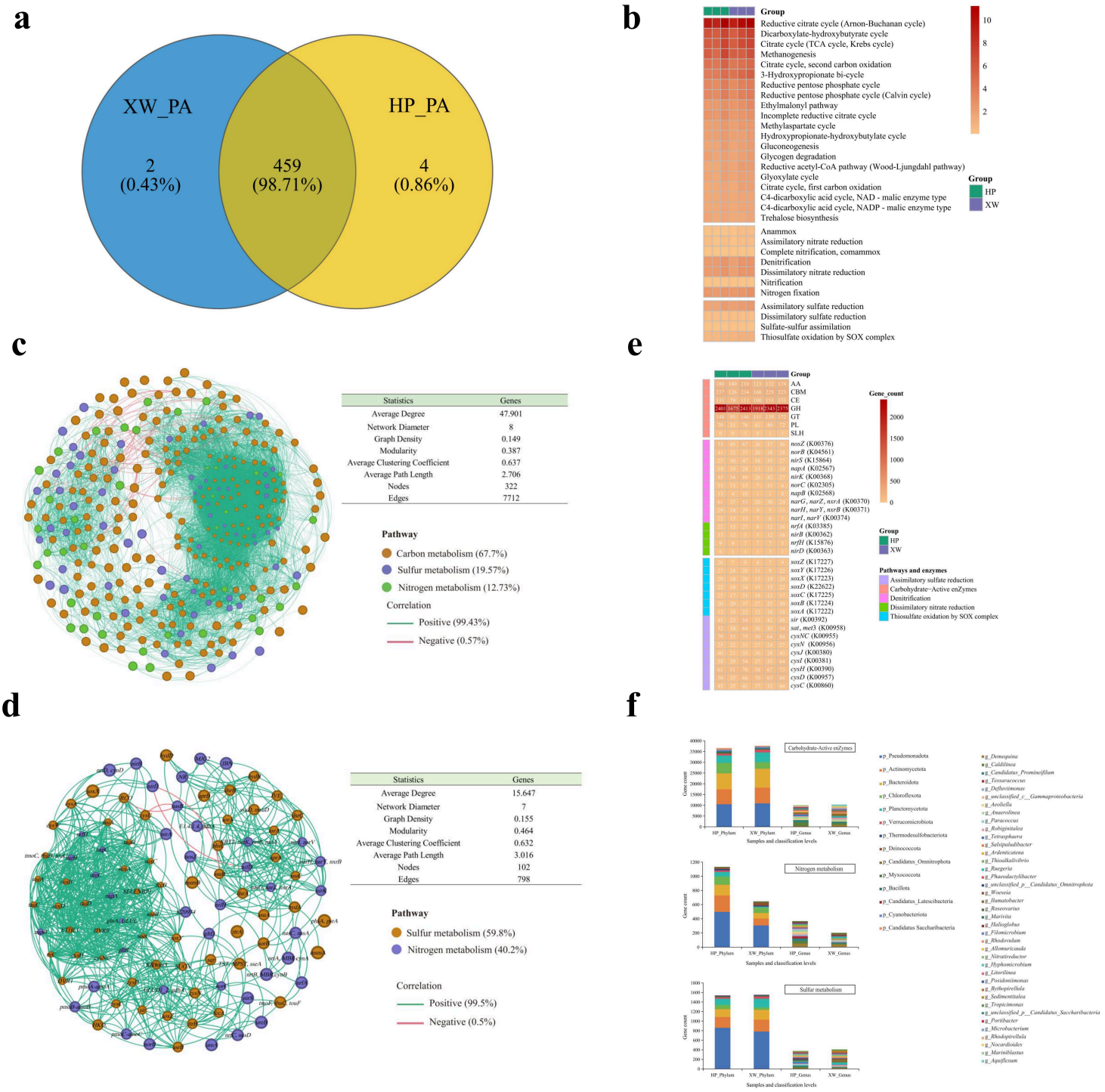

Figure 4

Functional analysis of particle-associated microbial communities in the ML stage. (a) Venn diagram showing shared and unique KEGG pathways between XW and HP samples. (b) Heatmap depicting the relative abundance of metabolic pathways involved in carbon, nitrogen, and sulfur metabolism. (c) Co-

occurrence network of genes associated with carbon, nitrogen and sulfur metabolism (n ≥ 6, |r| > 0.8, p < 0.05). (d) Co-occurrence network of genes specific to nitrogen and sulfur metabolism (n ≥ 6, |r| > 0.8, p < 0.05). (e) Heatmap of the relative abundance of genes encoding carbohydrate-active enzymes and those involved in nitrogen and sulfur metabolism. (f) Taxonomic attribution of bacteria involved in carbohydrate-active enzymes, nitrogen, and sulfur metabolism.

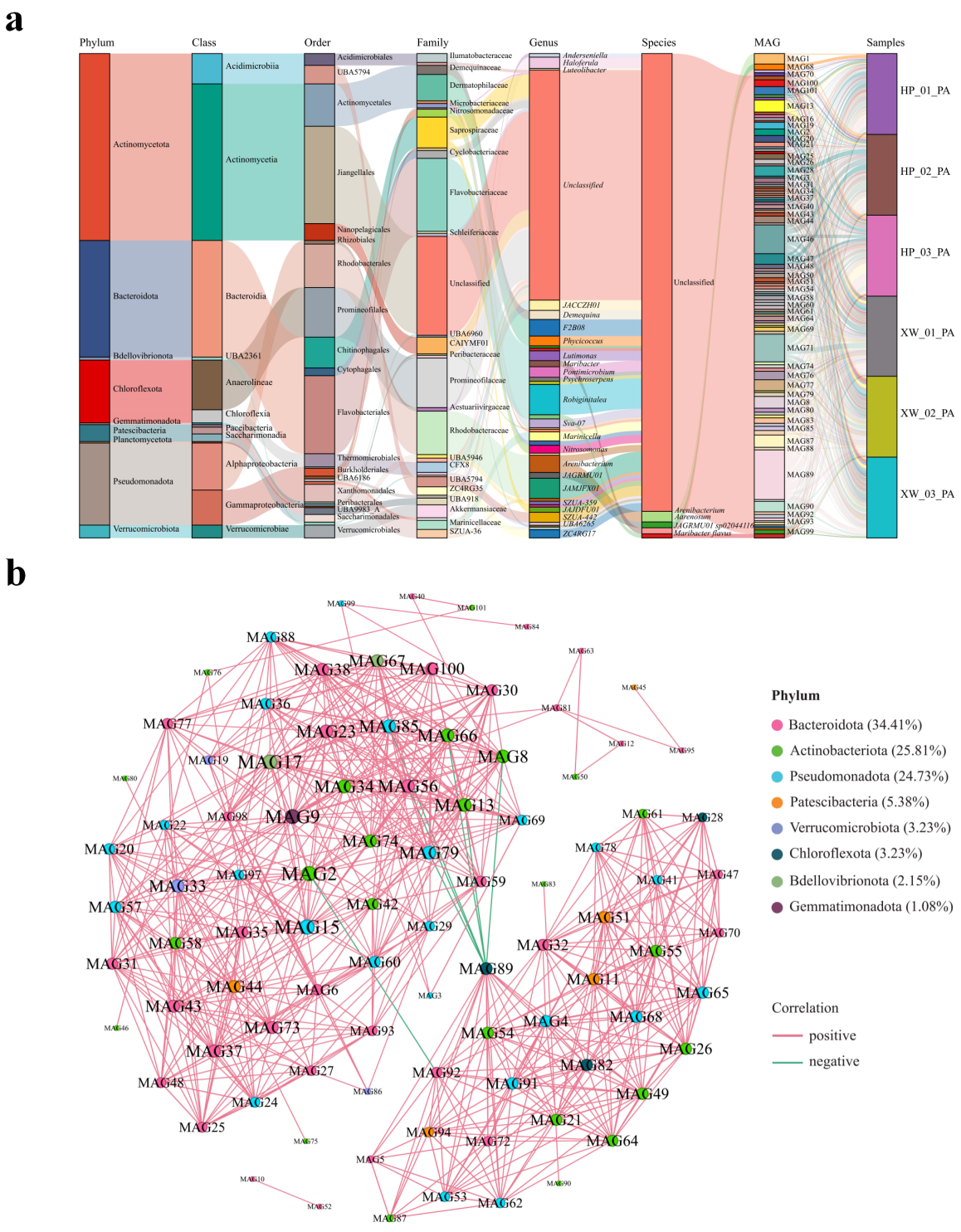

Figure 5

Taxonomic profiling and interaction networks of reconstructed MAGs. (a) Sankey diagram illustrating the taxonomic composition and distribution of MAGs across different levels. (b) Co-occurrence network depicting the associations among different MAGs.

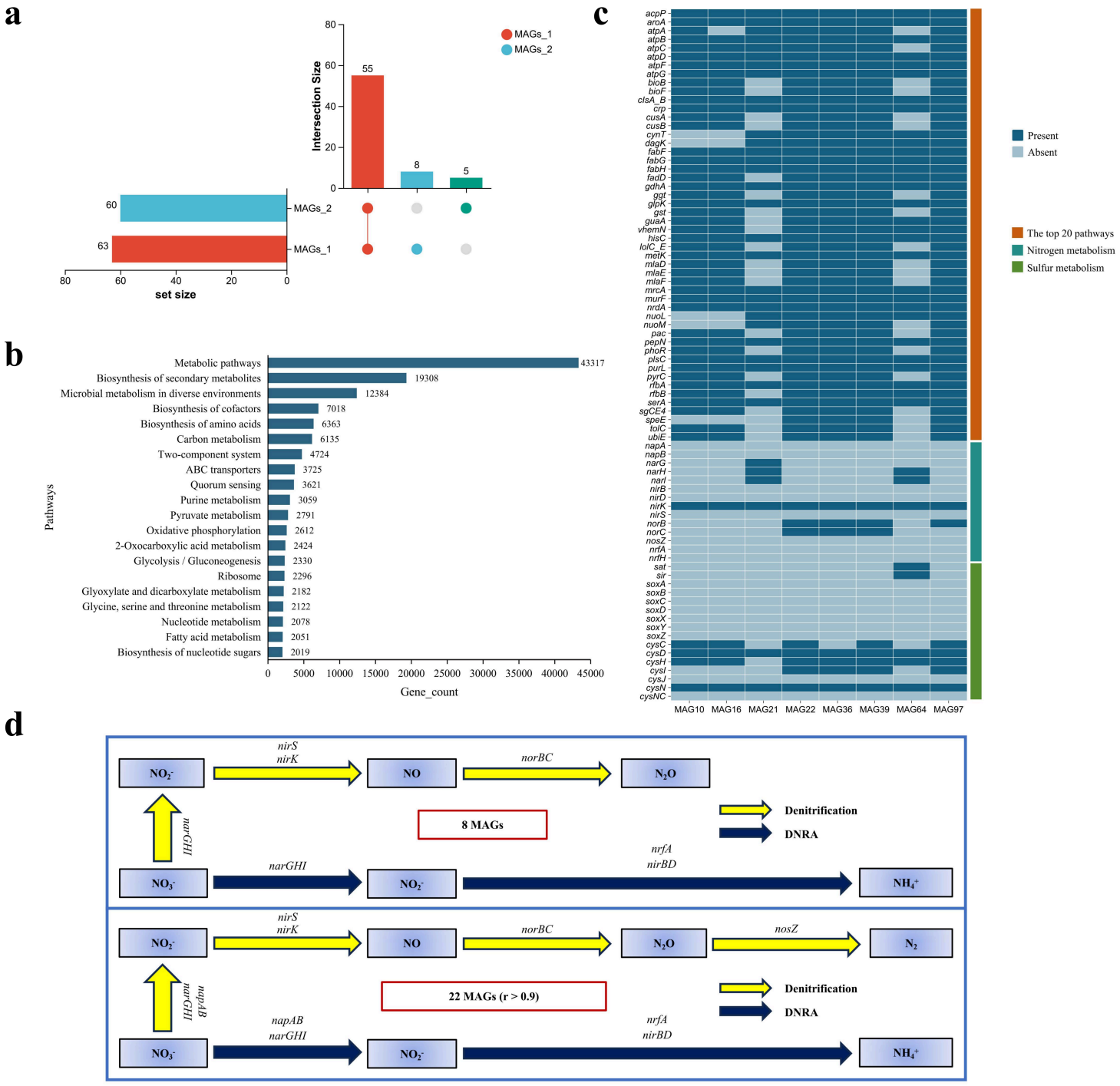

Figure 6

Functional profiling of reconstructedMAGs. (a) UpSet plot of prevalent and abundant MAG lineages. (b) Top 20 enriched metabolic pathways. (c) Presence or absence of genes for the top 20 pathways and key nitrogen and sulfur metabolism genes across the eight core MAGs. (d) Simplified diagram of the nitrogen metabolism pathway in the eight core MAGs and 22 highly correlated MAGs (r > 0.9).

Supplementary Files

This is a list of supplementary files associated with this preprint. Click to download.

- SupplementaryTables.csv